

SEISMOLOGY OF A LARGE SOLAR CORONAL LOOP FROM EUVI/*STEREO* OBSERVATIONS OF ITS TRANSVERSE OSCILLATION

E. VERWICHTE¹, M. J. ASCHWANDEN², T. VAN DOORSSELAERE¹, C. FOULLON^{1,3}, AND V. M. NAKARIAKOV¹

¹ Centre for Fusion, Space and Astrophysics, Department of Physics, University of Warwick, Coventry CV4 7AL, UK; Erwin.Verwichte@warwick.ac.uk

² Lockheed Martin Advanced Technology Center, Solar and Astrophysics Laboratory, Organization ADBS, Building 252, 3251 Hanover Street, Palo Alto, CA 94304, USA

³ Mullard Space Science Laboratory, University College London, Dorking, UK

Received 2008 November 11; accepted 2009 March 26; published 2009 May 20

ABSTRACT

The first analysis of a transverse loop oscillation observed by both *Solar Terrestrial Relations Observatories (STEREO)* spacecraft is presented, for an event on the 2007 June 27 as seen by the Extreme Ultraviolet Imager (EUVI). The three-dimensional loop geometry is determined using a three-dimensional reconstruction with a semicircular loop model, which allows for an accurate measurement of the loop length. The plane of wave polarization is found from comparison with a simulated loop model and shows that the oscillation is a fundamental horizontally polarized fast magnetoacoustic kink mode. The oscillation is characterized using an automated method and the results from both spacecraft are found to match closely. The oscillation period is 630 ± 30 s and the damping time is 1000 ± 300 s. Also, clear intensity variations associated with the transverse loop oscillations are reported for the first time. They are shown to be caused by the effect of line-of-sight integration. The Alfvén speed and coronal magnetic field derived using coronal seismology are discussed. This study shows that EUVI/*STEREO* observations achieve an adequate accuracy for studying long-period, large-amplitude transverse loop oscillations.

Key words: magnetic fields – MHD – Sun: corona – Sun: oscillations

Online-only material: color figures, mp4 animations

1. INTRODUCTION

Magnetohydrodynamic (MHD) waves and oscillations are ubiquitous in the solar corona as is evident from the numerous observations using space-borne and ground-based instruments (e.g., Tomczyk et al. 2007). Transverse oscillations of coronal loops are of particular interest (e.g., Aschwanden et al. 1999; Nakariakov et al. 1999; Verwichte et al. 2004; De Moortel & Brady 2007). They are interpreted as fast magnetoacoustic kink oscillations (Nakariakov et al. 1999; Van Doorselaere et al. 2008b). Through the application of the technique of coronal seismology (for a review see Nakariakov & Verwichte 2005), they allow us to measure the coronal magnetic field (Nakariakov & Ofman 2001) and loop structuring (e.g., Andries et al. 2005; Dymova & Ruderman 2006; Díaz 2006; McEwan et al. 2008; Verth & Erdélyi 2008; Van Doorselaere et al. 2008a). Furthermore, because of the observed rapid damping, they provide a rich test bed for coronal wave theories such as resonant mode conversion (Ruderman & Roberts 2002; Arregui et al. 2008; Goossens et al. 2008) or wave leakage (Brady & Arber 2005; Mikhalyaev & Solov'ev 2005; Verwichte et al. 2006a, 2006b; Terradas et al. 2006).

Transverse loop oscillations have mainly been studied in imaging data from the *Transition Region And Coronal Explorer (TRACE)*; Aschwanden et al. 2002). Here, for the first time an observation of a transverse loop oscillation seen by the Extreme Ultraviolet Imager (EUVI) on board the two *Solar Terrestrial Relations Observatories (STEREO)* is analyzed. Admittedly, EUVI seems at first glance not to be best suited for studying such type of oscillations because of a spatial resolution three times lower than *TRACE* and a temporal resolution of 2.5 minutes. The typically observed period is 5 minutes and only in a few cases are there reports of periods above 10 minutes (Aschwanden et al. 2002; Foullon et al. 2005).

However, contrary to *TRACE*, EUVI observes the full disk and will be able to see all events within the detectable parameter range. Also, the combination of images from two different perspectives allows for the three-dimensional investigation of oscillating coronal structures (Aschwanden et al. 2008). An improved determination of the loop length will reduce the error in the seismological determination of the coronal magnetic field. Lastly, two viewpoints can help to minimize errors in density measurements from line-of-sight background subtraction.

Section 2 introduces the EUVI observations and the oscillating loop event. In Section 3, the method to determine the three-dimensional geometry of the loop is explained and applied. Also, the polarization of the observed loop oscillation is examined. In Section 4, the oscillation time series are analyzed in detail. Finally, in Section 5 the results are discussed.

2. OBSERVATIONS

The active region NOAA 10962 is studied on 2007 June 27 between 17:30 and 18:50 UT using the EUVI instrument. It is part of the Sun Earth Connection Coronal and Heliospheric Investigation (SECCHI) instrument package (Wülser et al. 2004; Howard et al. 2008) on board the two *STEREO* spacecraft, Ahead (A) and Behind (B). These two spacecraft observe the Sun from two different vantage points along the Earth orbit. At the date of the observation, they were separated by $15^\circ 4$. The two spacecraft are only a few degrees above the ecliptic plane. Therefore, the separation in longitude is similar, i.e., $15^\circ 2$. EUVI takes full disk images approximately every 2.5 minutes in the EUV 171 Å bandpass, which is sensitive to coronal plasmas with temperatures of around 0.9 MK. The CCD image pixel size is $1''.59$. Because *STEREO A & B* are at different distances from the Sun, 0.96 and 1.08 AU, the projected distance on the Sun of one pixel is 1100 and 1240 km, respectively. The *STEREO B* data are rescaled and aligned to match *STEREO A*. *STEREO B* takes

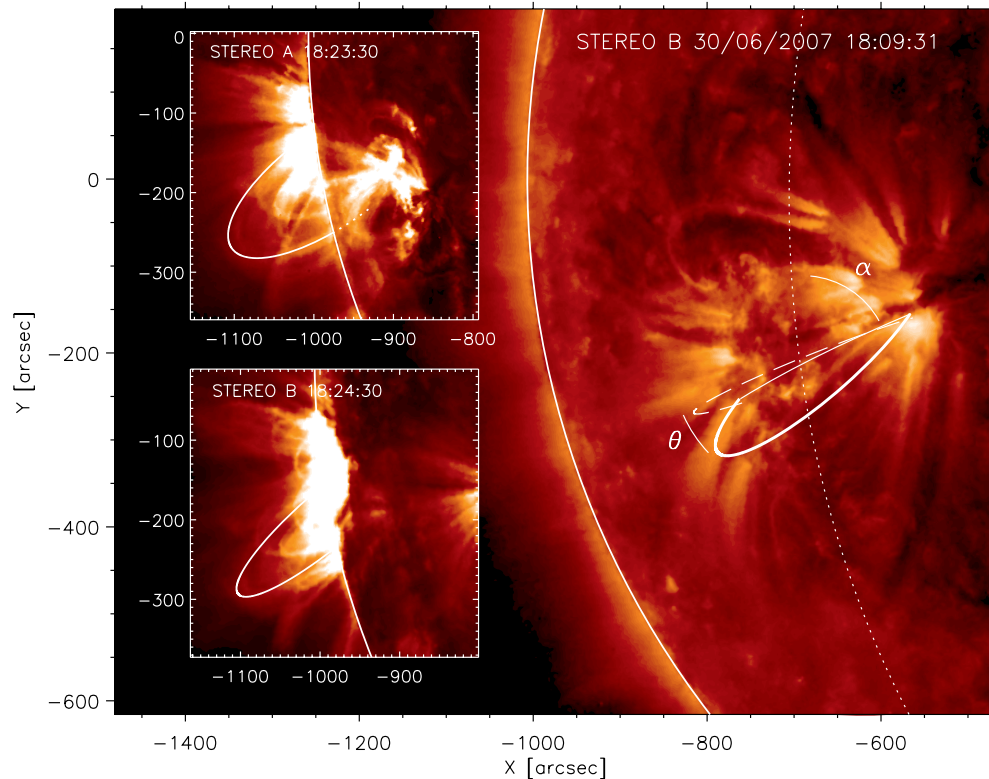


Figure 1. Determination of the three-dimensional loop geometry using forward modeling of a semicircular loop (thick solid line). The footpoints are identified in a *STEREO-B* image on June 30. The thin solid line is the loop base line at the solar surface connecting the footpoints. The dashed line is the semicircular loop with zero inclination. The azimuth and inclination angles, α and θ , are shown. The insets show the loop model superimposed on the observations of June 27 from both spacecraft. The dotted line refers to a loop section behind the solar limb. The angular scales used are measured relative to *STEREO A*.

(A color version of this figure is available in the online journal.)

observations with a 1 minute delay compared with *STEREO A* to compensate for the difference in light travel time from the Sun to the spacecraft. For this observation no complementary data from *TRACE* or *Hinode* is available.

NOAA 10962 is an old, extended active region in which the magnetic surface fluxes of opposite polarities are well separated by approximately 10° in longitude (McIntosh classification Axx). Hence, the coronal loops in the active region have a simple bipolar structure with the loop arcade axis orientated north south (see Figure 1). The active region is seen on the east solar limb in both instruments. *STEREO B* has the most favorable viewing angle of both the spacecraft. Between 17:49 and 18:03 UT GOES recorded a C1.3 class flare from the active region (also seen by *RHESSI*). This flare perturbs the active region and a transverse oscillation is excited in the southern part of the loop arcade. In particular, a bundle of loops oscillates collectively with a period of around 10 minutes and which remains visible for roughly three oscillation periods, as seen in Figure 2. We shall study this oscillation in detail. From now on we shall for simplicity denote the loop bundle as a loop.

3. LOOP GEOMETRY

The main advantage of the *STEREO* mission is the ability to perform a three-dimensional reconstruction of coronal and heliospheric structures. For seismological purposes the loop length and the loop plane are of primary interest. Therefore, we decide to fit a semicircular model to the observed loop. Such a loop model depends on five parameters: longitude and latitude of the circle center, loop radius, R , azimuth angle between loop footpoints and north south line, α , and the loop

plane inclination with respect to the solar surface, θ . Fixing the location of the footpoints constrains all parameters except for the loop inclination. This angle is determined by forward modeling the semicircular loop in both *STEREO* images for varying inclination angles and matching it with the observations by eye. However, because the loop is seen over the limb in both spacecraft, the loop footpoints cannot be located in the images with any degree of accuracy. This hampers a direct reconstruction using the technique outlined in Aschwanden et al. (2008). Instead of systematically scanning all possible footpoint locations, we propose to make an informed guess of the likely location of the footpoints by looking at a *STEREO B* image of the same active region taken three days later (see Figure 1). The same loop is not visible but we assume that the global basic magnetic topology of the active region remains similar, with footpoints of loop bundles seen then as candidate locations. A guess set of footpoints is selected and their coordinates transformed (rotated) to the situation three days earlier. It is then verified if a match can be found between the loop model based on these footpoints and the observed loop. If no satisfactory match is found, new footpoints are selected and the process is repeated. In this fashion, a loop model was fitted to the loop observed by both *STEREO* spacecraft. The loop parameters found are $R = 110$ Mm, $\alpha = 71^\circ$ measured from north clockwise and $\theta = 27^\circ$ southward with respect to the solar surface normal. In order to clearly show the loop geometry, the loop is shown in Figure 1 as would have appeared three days later on disk.

Because the loop length, $L (= \pi R)$, is an important physical quantity for the seismological interpretation of the loop oscillation, the error on L is estimated by repeating the footpoint selection process multiple times in an area equal to the size of a

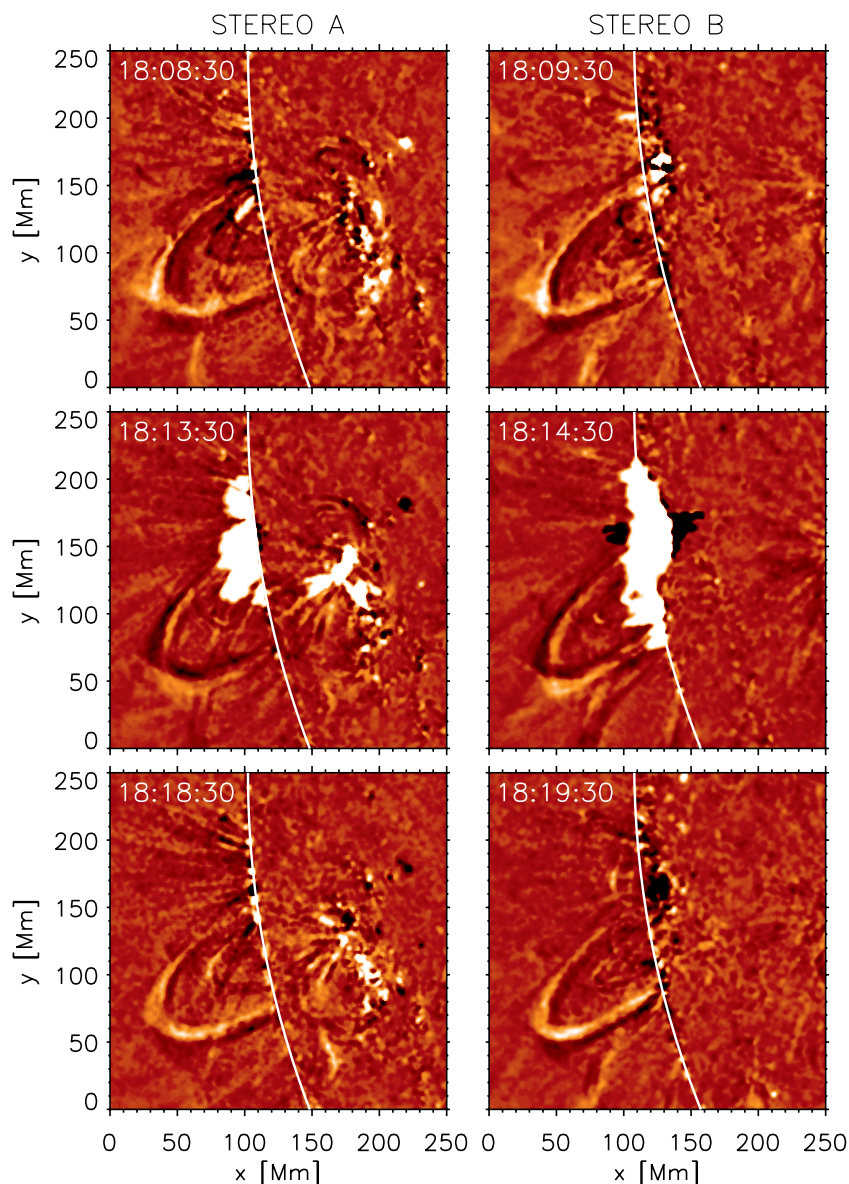


Figure 2. Difference images for three times and for *STEREO A* (left) and *STEREO B* (right). The difference image is constructed as the difference between the image at the given time and the image 5 minutes earlier.

(A color version of this figure is available in the online journal.)

local arcade footpoint, i.e. about 30 arcsec wide. The standard deviation of the found values is used as an estimate of the error on the loop length. Thus, the loop length is determined to be $L = 340 \pm 15$ Mm. The relative error on the loop length is 4%. Any departures of the true loop shape from semicircular is of course not included in the error estimates. But since Nakariakov & Ofman (2001) this source of error is known to be relatively unimportant.

The robustness of the reconstruction method used here has been verified by an independent three-dimensional reconstruction using a stereoscopic triangulation method that is not constrained to a semicircular model and which was developed after submission of this paper (Aschwanden 2009). In this method, both *STEREO* images are aligned such as to make the horizontal direction lie in the epipolar plane (determined by the Sun and the *STEREO* spacecraft). Thus, the same (epipolar) point in both images has the same vertical coordinate in each image. The three-dimensional loop coordinates of each point are determined from the measurement of the horizontal parallax.

Nine epipolar loop points have been selected and the loop is reconstructed using a cubic spline fitting. The parameter values found using this method are consistent with those deduced above (even though there are expected differences in the detailed loop shape). In particular, the determination of the loop length, which is an important ingredient for seismological derivations, is confirmed. Comparison between the semicircular loop model and this method explained below suggests that the loop length error is around 10%.

Using the reconstructed loop geometry we can simulate how a kink mode appears in the difference images, depending on its mode of polarization and its harmonic (Wang & Solanki 2004). Figure 3 shows a simulated difference image for horizontally and vertically polarized fundamental modes ($n = 1$) and their second harmonic ($n = 2$). We compare the simulated images with Figure 2. The observed oscillation mode reveals a typical brightness pattern in the difference images: opposite brightness between the inner and outer edges as well as between the two loop legs. The fundamental horizontally polarized kink mode

Table 1
Oscillation Parameters

Instruments	t_0	ξ_0 (Mm)	V_0 (km s $^{-1}$)	P (s)	τ (s)	ϕ ($^\circ$)
A	18:01	4.0 ± 1.1	39 ± 13	642 ± 29	869 ± 366	111 ± 13
B	18:02	3.6 ± 1.3	36 ± 15	627 ± 32	1494 ± 723	111 ± 16
A+B		3.8 ± 0.9	37 ± 10	635 ± 22	880 ± 297	111 ± 11
A	18:01	3.9 ± 1.0	38 ± 13	636 ± 40	920 ± 338	107 ± 14
B	18:02	3.2 ± 1.0	33 ± 12	616 ± 42	1112 ± 524	105 ± 20
A+B		3.6 ± 0.7	35 ± 9	626 ± 29	976 ± 312	106 ± 12

Notes. The first three rows are the results from a single fit. The last three rows are the result from a randomization technique.

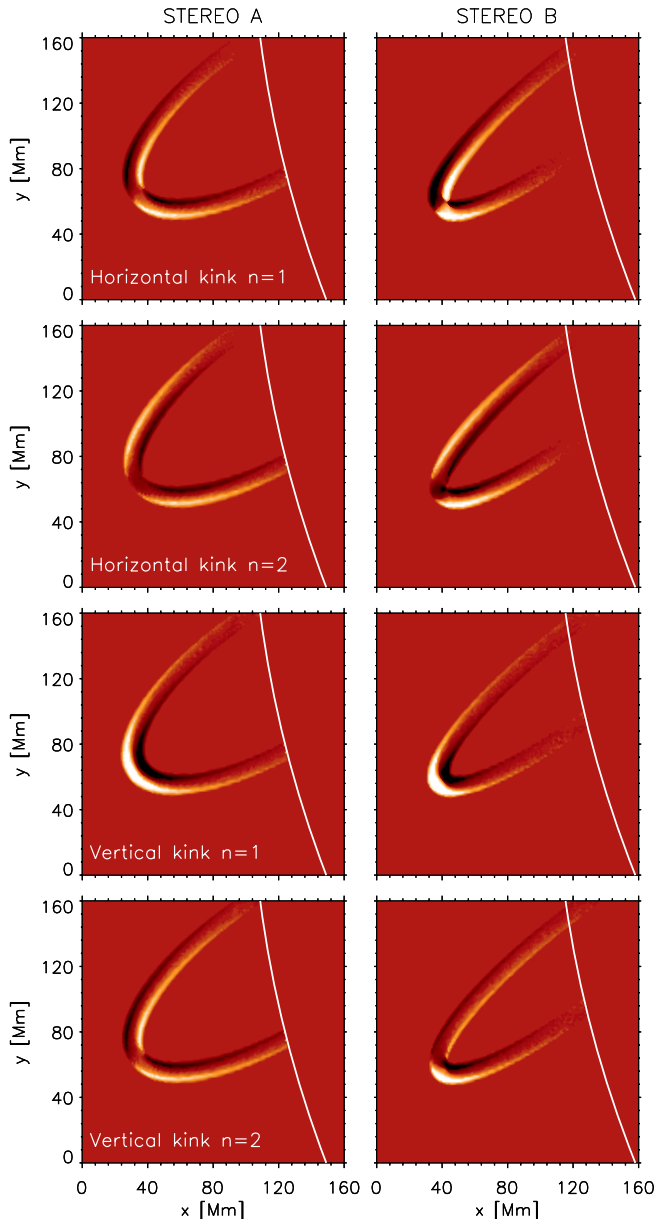


Figure 3. Simulated difference images for the modeled loop as seen in both *STEREO* spacecraft for various modes of oscillation: fundamental horizontally polarized mode (top), second horizontally polarized harmonic (second row), fundamental vertically polarized mode (third row), and the second vertically polarized harmonic (bottom). (A color version of this figure is available in the online journal.)

and the vertically polarized second harmonic kink mode can reproduce this pattern. However, the fundamental horizontal mode is the more likely candidate from visual inspection of the

data movie. The movies available in the online journal compare the simulated loop oscillation with the observations in both *STEREO* viewpoints for the fundamental horizontally polarized mode (movie 1) and the second vertically polarized harmonic (movie 2). Additional reasons will be given in Section 5.

4. ANALYSIS OF THE OSCILLATION

For each data set, the relevant parameters describing the loop oscillation are determined automatically in the following manner. A linear path is taken that is centered on the loop top and parallel with the projected direction of polarization of the loop oscillation as determined from the simulation discussed above (see Figure 4). Note that the projected direction is approximately along the loop axis. The data are then averaged over the path width (9 pixels wide). In the resulting intensity profile, the location of the loop top is determined by fitting a Gaussian. The path profiles and the loop top locations as a function of time are shown in Figure 5. Next, from the time series of the loop top locations, a quadratic trend is subtracted, which yields the time series of the projected loop top displacement, $\xi_{\text{proj}}(t)$. Because the angle of the loop plane with respect to the plane of the sky is known, the real loop top displacement $\xi(t)$ is calculated to be $\xi(t) = \xi_{\text{proj}}(t) / \cos \chi$, where χ is the angle between the loop plane normal and the plane of the sky and is equal to 23° and 14° for *STEREO A* and *B*, respectively.

The loop top displacement time series is fitted by a damped oscillation of the form $\xi(t) = \xi_0 \exp(-(t - t_0)/\tau) \cos(2\pi(t - t_0)/P + \phi)$, where the fitting parameters ξ_0 , P , τ , and ϕ are the displacement amplitude, oscillation period, e -folding damping time, and phase, respectively. The start time of the fit, t_0 , is set equal to 18:01 and 18:02 UT for *STEREO A* and *B*, respectively. The velocity amplitude corresponding to the displacement amplitude is $V_0 = 2\pi\xi_0/P$. For the fit a displacement error is included that corresponds to the maximum between the error of the Gaussian loop top localization and the distance corresponding to one instrument pixel size (which slightly differs between *STEREO A* and *B*). The fit is performed using a Levenberg Marquardt least-squares minimization technique (Moré & Wright 1993), implemented in the Interactive Data Language by Markwardt (2008). The errors on the fitting parameters are the formal 1σ errors computed from the covariance matrix. The fitted profiles are shown in Figure 5 and the determined oscillation parameters are listed in Table 1. Both instruments (viewpoints) give a mutually consistent answer. Therefore, the measured oscillation parameters are rms-averaged (also shown in Table 1), which reduces the error.

The found parameter errors are similar to studies with *TRACE*. In order to compare the obtained parameter accuracy with studies such as Van Doorselaere et al. (2007), the parameter values and errors are also estimated using a randomization

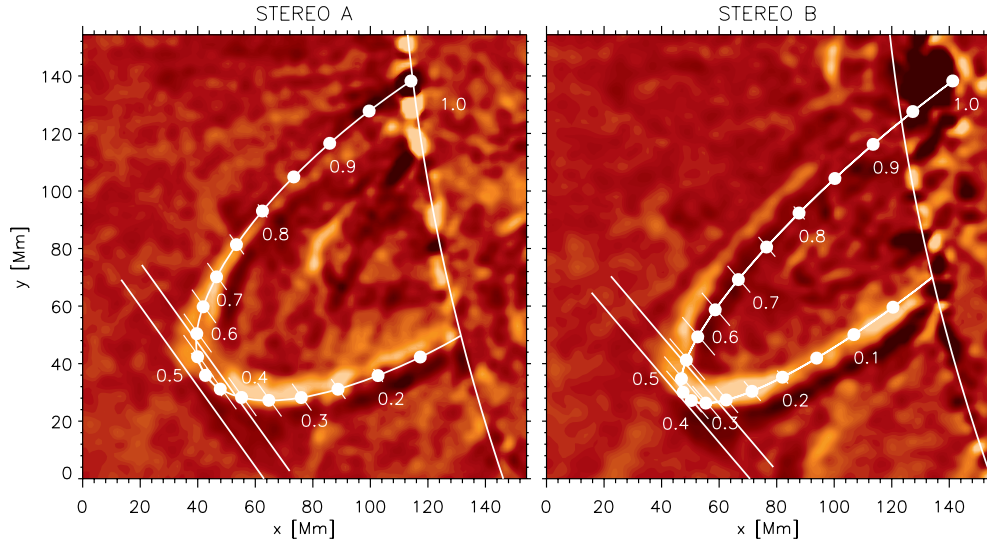


Figure 4. Simulated loop is shown in more detail superimposed on a difference image from each *STEREO* spacecraft. The dots mark out the distance along the loop in steps of 0.05 times the loop length. The lines through the dots show the projected direction of the fundamental horizontally polarized kink mode. The two parallel lines outline path used in the oscillation analysis, which is centered on the loop top and parallel to the projected direction of oscillation polarization. (A color version of this figure is available in the online journal.)

technique. To each measurement in the time series, a Gaussian noise is added with a sigma equal to the displacement error. A least-squares fit is performed on the new time series and the fitting parameters determined. This process is repeated 200 times. The resulting distribution of parameter values is shown for *STEREO A* in Figure 6, which shows a distinct peak in all four parameters. The result is similar for *STEREO B* (not shown). A Gaussian is fitted to the distribution. The location and width of the Gaussian are then taken to be the parameter value and error, respectively. Table 1 shows these values. Both parameter values and errors are consistent with the single fit result.

To summarize, the loop oscillates approximately at a period of 630 ± 30 s with a damping time of 1000 ± 300 s. The oscillation quality factor is $\tau/P = 1.6 \pm 0.5$. The displacement amplitude is 4 Mm. The damped oscillator fits the displacement time series well for approximately the first 2.5 periods. After that the displacement data does not show oscillatory behavior and the fitted curve falls within the error bars. However, as Figure 7 shows, the oscillation can be traced for up to five periods in the intensity at the loop top. The damped oscillation curve found from fitting the displacement has been overlaid with an arbitrary amplitude and shows that the intensity variations follow it well.

5. DISCUSSION

From the measured oscillation period and loop length, and assuming a fundamental mode, the longitudinal phase speed of the wave mode is found to be $V_{\text{ph}} = 2L/P = 1100 \pm 100$ km s⁻¹. This value of phase speed is consistent with previous observations of transverse loop oscillations (e.g., Verwichte et al. 2004). MHD wave theory shows that a fast magnetoacoustic kink mode in a cylindrical loop model and in the long wavelength and zero plasma- β limits has a phase speed equal to the kink speed, C_K (Edwin & Roberts 1983):

$$C_K = \sqrt{\frac{2}{1 + \rho_e/\rho_i}} V_A = \sqrt{\frac{2}{\mu_0(\rho_i + \rho_e)}} B, \quad (1)$$

where V_A is the Alfvén speed and B is the magnetic field strength in the loop. μ_0 is the permeability of free space, ρ_i and ρ_e are the mass densities of the loop and the external plasma, respectively. In this observation, the observed oscillation occurs in a bundle of loops rather than in a single loop. Recent theoretical and numerical studies have shown that the global kink mode still exists in models with multiple loops (Luna et al. 2008; Van Doorselaere et al. 2008d; Terradas et al. 2008). The single loop model is robust and can be applied if the internal density is replaced by the average density of the loop bundle $\langle \rho_i \rangle = f\rho_i$, where f is an undetermined filling factor. The density ratio $\rho_e/\langle \rho_i \rangle$ is crudely estimated from the intensity enhancement due to the loop relative to the background intensity as follows:

$$\frac{\Delta I}{I_0} \approx \frac{((\rho_i^2) - \rho_e^2) 2a}{\rho_e^2 \Delta L}, \quad (2)$$

where I_0 is the line-of-sight-integrated intensities from the background next to the loop, $2a$ ($=10$ Mm) is the line-of-sight depth of the loop, and ΔL is the typical line-of-sight depth from which the majority of emission is originating. Because there is no other active region in front or behind the line of sight besides that of the oscillating loop, it is reasonable to assume that the majority of the emission comes from the active region. The region dimensions are of the order of the loop length, i.e., we take ΔL between $0.5L$ and $2L$. We have also assumed that the plasma is isothermal. The intensity ratio is found to be equal to 0.9. The density ratio from Equation (2) is found to be roughly equal to

$$\frac{\rho_e}{\langle \rho_i \rangle} \approx \frac{1}{\sqrt{1 + \frac{\Delta I}{I_0} \frac{\Delta L}{2a}}} \approx 0.1-0.3. \quad (3)$$

The Alfvén speed is found using Equation (1), with the density ratio in the previously deduced range, to be $V_A = 800 \pm 100$ km s⁻¹. The minimum value of the Alfvén speed is for a zero density ratio and is equal to $V_A = 760 \pm 70$ km s⁻¹.

If the observed oscillation is the second vertically polarized harmonic kink overtone, with a wavelength equal to L , the Alfvén speed would be around 400 km s⁻¹. This would imply a

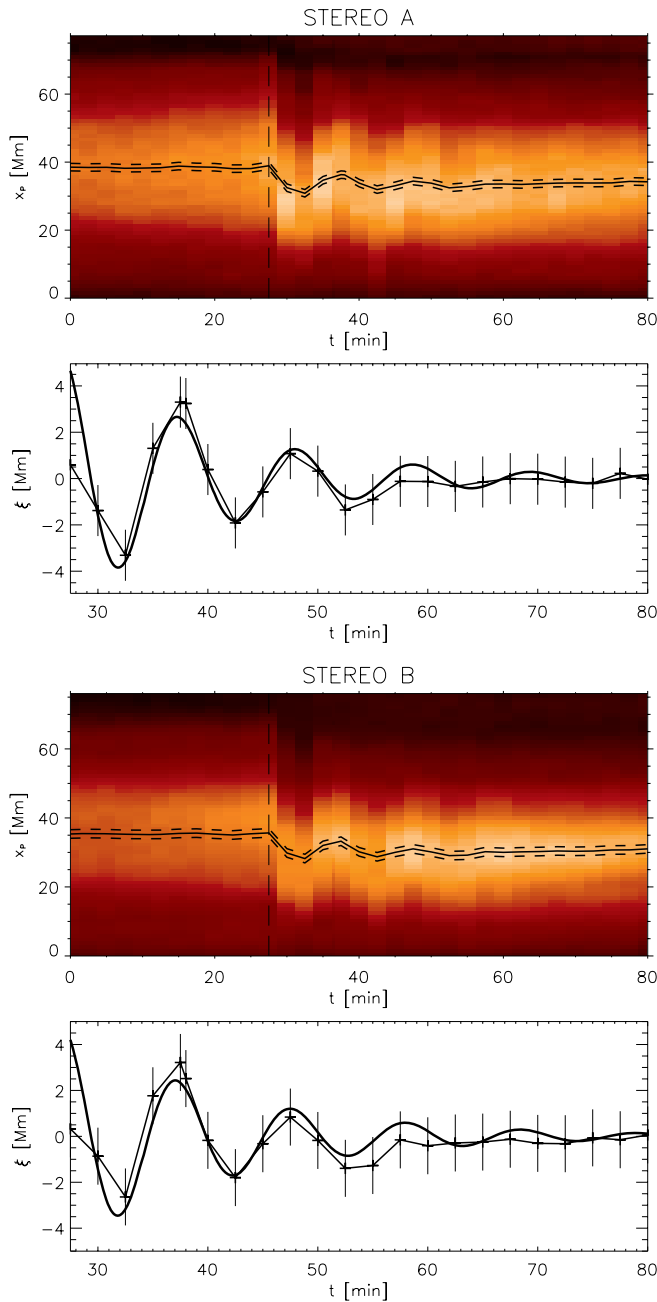


Figure 5. For each *STEREO* spacecraft, a pair of figures is shown. The top figure shows the intensity profiles of the selected path as a function of time and projected distance, x_p , along the path. The solid line is the center position of the fitted Gaussian profile. The dashed lines indicate the error. The vertical long-dashed line shows the time when the loops are first perturbed. The bottom figure shows the detrended loop top displacement as a function of time with a fitted damped oscillation superimposed. The time for *STEREO B* has been corrected for light travel time with respect to *STEREO A*.

(A color version of this figure is available in the online journal.)

plasma- β of about 20%, which is rather high. Therefore, we use this as an additional argument to choose the observed oscillation to be the fundamental horizontally polarized kink mode instead.

Furthermore, the coronal loop density is estimated using the EUVI 171 Å response function (Aschwanden et al. 2008). We assume that the observed emission is at the peak temperature of the 171 Å bandpass, i.e., 0.9 MK. Therefore, the measured density can be considered to be a lower limit. Following Aschwanden

et al. (2008) the emission measure is calculated as $EM = (I - I_0)/(q_{171} R_{171})$, where $q_{171} = 1.32 \text{ ph DN}^{-1}$ is the photons to data numbers conversion factor and $R_{171} \approx 3500 \text{ ph m}^3$ is the value of the EUVI 171 Å bandpass response function at $T = 0.9 \text{ MK}$. From the emission measure, the electron number density is calculated as $fn_e = (EM/wS)^{1/2} = (6.7 \pm 0.5) 10^{14} \text{ m}^{-3}$, where $S = 1.2 \times 10^{12} \text{ m}^2$ is the surface area covered by one EUVI CCD pixel and w is the line-of-sight integration depth of the loop, which we assume to be approximately equal to $2a$. However, during the oscillation this depth varies as the loop geometry changes. These variations are taken into account for the estimation of the error on the density. The average loop mass density is expressed in terms of n_e using the coronal value of the mean coronal molecular mass $\bar{m} = 1.16$ such that $\langle \rho_i \rangle = \bar{m} m_p n_e$ with m_p the proton mass.

The average magnetic field in the loop, B , is estimated from the definition of the kink speed to be

$$B = 11.1 \left(1 + \frac{\rho_e}{\langle \rho_i \rangle}\right)^{1/2} \left(\frac{V_{\text{ph}}}{10^6 \text{ m s}^{-1}}\right) \left(\frac{fn_e}{10^{15} \text{ m}^{-3}}\right)^{1/2} \\ G = 11 \pm 2 \text{ G.} \quad (4)$$

The relative error of the magnetic field strength is about 20%. The magnetic field strength of $11 \pm 2 \text{ G}$ is consistent with values found in previous seismological studies (Nakariakov & Ofman 2001; Verwichte et al. 2004; Van Doorselaere et al. 2007, 2008c). In particular, Van Doorselaere et al. (2007) observed an oscillation with a period of 440 s in a 400 Mm long loop. They deduced a magnetic field strength of 10–14 G.

If we use an error of the loop length of 10% instead, we find the magnetic field strength to be $11 \pm 3 \text{ G}$.

If we assume that the physical mechanism responsible for the oscillation damping is resonant mode conversion, using Equation (73) of Ruderman & Roberts (2002), we deduce from the measured oscillation quality factor and density contrast that the ratio of the thickness of the inhomogeneous layer over the typical half-width of each constituent loop of the loop bundle (assuming they do not differ significantly from each other),

$$\frac{\ell}{a} = \frac{2 \langle \rho_i \rangle + \rho_e}{\pi \langle \rho_i \rangle - \rho_e} \frac{P}{\tau} = 0.4 \pm 0.2. \quad (5)$$

In this study, clear intensity variations associated with transverse loop oscillations are reported for the first time. There have been a few reports of intensity variations that have been interpreted as fast magnetoacoustic kink modes, but these were not conclusive either due to the absence of simultaneous measurements of intensity and displacement or velocity variations (Williams et al. 2001; Cooper et al. 2003; O’Shea et al. 2007) or due to the absence of a clear oscillation pattern in intensity (Wang & Solanki 2004). We do not expect our intensity variations to be caused by variations in density or temperature, as these are theoretically predicted to be small for linear horizontally polarized fast magnetoacoustic kink oscillations and involve density enhancements as well as depletions that in the line-of-sight integration tend to cancel each other (e.g., Van Doorselaere et al. 2008b). The vertically polarized kink oscillation may have intensity variations caused by the change of the loop cross section, across which the Alfvén speed varies with height (Verwichte et al. 2006a). However, these modes have been discounted earlier. Additionally, the intensity variations are observed at the loop top, which would be inconsistent with the second vertical harmonic which has a node there. Terradas &

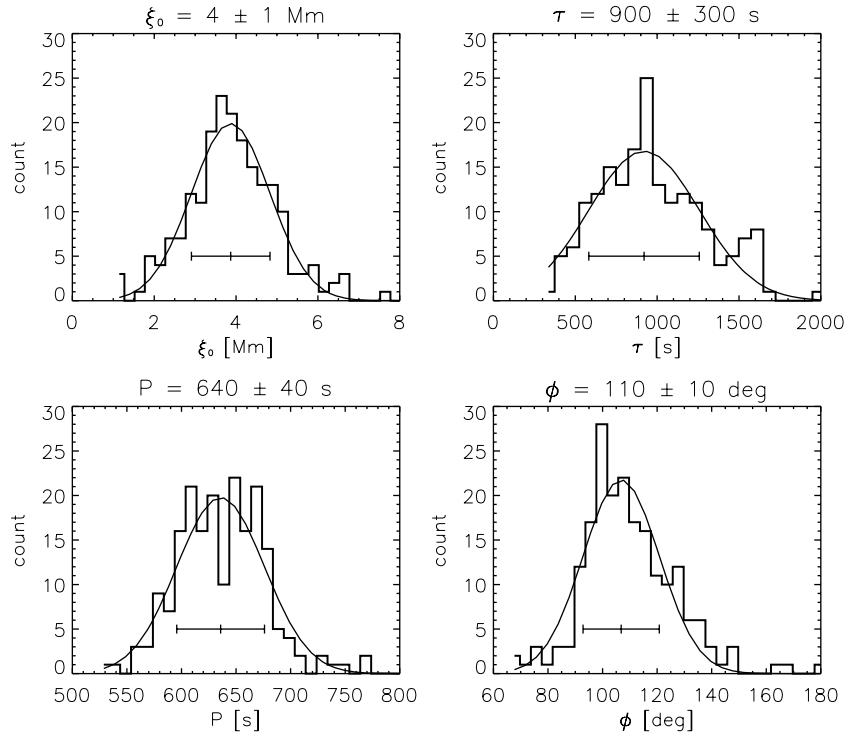


Figure 6. Distribution of the values of the four parameters of the damped oscillator fit to the 200 times randomized displacement time series from *STEREO A*. The distributions are fitted with a Gaussian. The location of the peak and the width of the Gaussian are shown.

Ofman (2004) studied intensity variations of transverse loop oscillations arising from the nonlinear ponderomotive force. However, such variations manifest themselves on a slower acoustic timescale than the observed oscillations. The intensity variations are most likely due to changes in the line-of-sight integration depth of the loop as the loop inclination varies (Cooper et al. 2003). This is confirmed by analyzing the intensity variations of the loop in the simulated images (as shown in Figure 3) in the same manner as the observations. Figure 7 shows that the simulated intensity variations are in phase with the displacement (here, it is in phase with the fitted displacement curve, which has been used as input for the time variation in the simulation). This type of intensity variations may be used for seismological purposes, i.e., infer loop thickness or substructuring. This is beyond the scope of the present paper.

We compare the measured oscillation period and displacement amplitude with the instrument's temporal and spatial resolution. With a time cadence of $\Delta t = 2.5$ minutes and a period of 630 s, $P/\Delta t = 4.2$. With a spatial pixel size of $\Delta x = 1.1$ Mm and a displacement amplitude of 4 Mm, $\xi_0/\Delta x = 3.5$, which means that the oscillation is visible in a range of 7 EUVI pixels. These numbers compare favorably with resolutions from previous studies using *TRACE*. In particular, for transverse loop oscillations studied by Nakariakov et al. (1999) and Verwichte et al. (2004), we find ratios of $P/\Delta t = 3.4$, $\xi_0/\Delta x = 5.6$, and $P/\Delta t = 10$ 15, $\xi_0/\Delta x = 1.4$, respectively. This shows that the oscillation studied here is resolved by EUVI as well as in previous studies by *TRACE*. Therefore, EUVI/STEREO observations achieve an adequate accuracy for studying long-period, large amplitude transverse loop oscillations. In fact, if this event had been seen by *TRACE*, the expected ratios would be $P/\Delta t = 21$ and $\xi_0/\Delta x = 11$.

In summary, the first observation of a transverse loop oscillation using EUVI seen by both *STEREO* spacecraft is presented. It demonstrates that despite the lower spatial and temporal

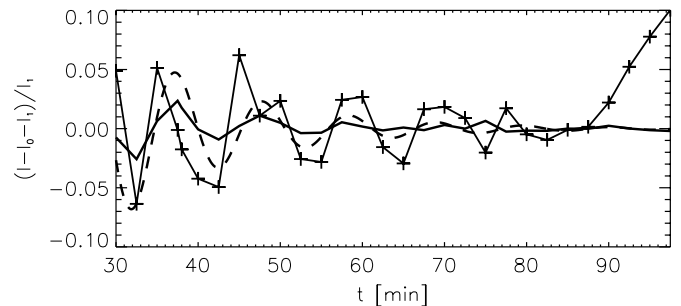


Figure 7. Relative intensity $(I - I_0 - I_1)/I_1$ at the position of the loop top as a function of time as seen by *STEREO A*. I_1 is the equilibrium loop intensity, which is calculated as a quadratic trend of $I - I_0$. The dashed curve is the damped oscillation that fits the displacement time series with the parameters for A+B listed in Table 1 but with an arbitrary amplitude. The thick solid line is the relative intensity at the position of the top of the loop in the simulated images.

resolution compared with *TRACE*, long-period transverse loop oscillations can be successfully studied with *STEREO*. The three-dimensional reconstruction made possible using both spacecraft allows for an improved measurement of the loop length ($L = 340 \pm 15$ Mm), which is an important quantity for the seismological investigation of loop oscillations. Also, the loop length obtained using a circular loop model is robust and deviates less than 10% from stereoscopic triangulations methods. Moreover, the reconstruction, combined with forward modeling, allows for an identification of the wave polarization, a capability absent with *TRACE*. This makes possible the correct selection of the image path orientation along which the loop displacement time series is measured. In earlier studies of transverse loop oscillations using *TRACE* the path has often been chosen to be perpendicular to the loop axis due to the lack of knowledge of the three-dimensional geometry (e.g., Aschwanden et al. 2002). When the true projected polarization direction differs significantly from perpendicular, as is the case here, a

perpendicularly orientated path would result in a distorted displacement time series. Consequently, this would increase the error on the oscillation parameters.

Using an automated scheme the oscillation parameters are determined from the transverse displacement time series, i.e., an oscillation period and damping time of 630 ± 30 s and 1000 ± 300 s, respectively. The results from both spacecraft are consistent. The oscillation is also detected in intensity, which is due to variations in the line-of-sight integration. By applying the technique of coronal seismology, the strength of the magnetic field in the oscillating loop is measured to be 11 ± 2 G, using an accurately measured loop length, a lower limit of the density and an estimated density contrast. Simultaneous EIS/*Hinode* observations would be needed to measure the loop density more accurately (Van Doorselaere et al. 2008c). Furthermore, observations of transverse loop oscillations on the disk could allow for the identification of the loop footpoints at the time of the oscillation and hence the application of a three-dimensional reconstruction using data from the two EUVI/*STEREO* instruments. However, large loops are relatively fainter compared with the background when seen on disk. For the above reasons, EUVI/*STEREO* observations of coronal loop oscillations will benefit from simultaneous EIS/*Hinode* and *TRACE* observations, as well as from future SDO observations.

E.V. acknowledges the financial support from the Engineering and Physical Sciences Research Council (EPSRC) Science and Innovation award. M.A. is supported by NASA *STEREO* under NRL contract N00173-02-C-2035. T.V.D. acknowledges the support from the Marie Curie Intra European Fellowship within the 7th European Community Framework Programme. C.F. acknowledges the financial support from the Science and Technology Facilities Council (STFC) on the MSSL and CFSA Rolling Grants. V.N. and M.A. acknowledge the support of the International Space Science Institute (ISSI) through its team Waves in the Solar Corona.

REFERENCES

- Andries, J., Goossens, M., Hollweg, J. V., Arregui, I., & Van Doorselaere, T. 2005, *A&A*, **430**, 1109
- Arregui, I., Terradas, J., Oliver, R., & Ballester, J. L. 2008, *ApJ*, **674**, 1179
- Aschwanden, M. J. 2009, *Space Sci. Rev.*, submitted
- Aschwanden, M. J., De Pontieu, B., Schrijver, C. J., & Title, A. M. 2002, *Solar Phys.*, **206**, 99
- Aschwanden, M. J., Fletcher, L., Schrijver, C. J., & Alexander, D. 1999, *ApJ*, **520**, 880
- Aschwanden, M. J., Wülser, J.-P., Nitta, N. V., & Lemen, J. R. 2008, *ApJ*, **679**, 827
- Brady, C. S., & Arber, T. D. 2005, *A&A*, **438**, 733
- Cooper, F. C., Nakariakov, V. M., & Tsiklauri, D. 2003, *A&A*, **397**, 765
- De Moortel, I., & Brady, C. S. 2007, *ApJ*, **664**, 1210
- Díaz, A. J. 2006, *A&A*, **456**, 737
- Dymova, M. V., & Ruderman, M. S. 2006, *A&A*, **459**, 241
- Edwin, P. M., & Roberts, B. 1983, *Solar Phys.*, **88**, 179
- Foullon, C., Verwichte, E., Nakariakov, V. M., & Fletcher, L. 2005, *A&A*, **440**, L59
- Goossens, M., Arregui, I., Ballester, J. L., & Wang, T. J. 2008, *A&A*, **484**, 851
- Howard, R. A., et al. 2008, *Space Sci. Rev.*, **136**, 67
- Luna, M., Terradas, J., Oliver, R., & Ballester, J. L. 2008, *ApJ*, **676**, 717
- Markwardt, C. 2008, Markwardt IDL Library, <http://cow.physics.wisc.edu/~craigm/idl/>
- McEwan, M. P., Díaz, A. J., & Roberts, B. 2008, *A&A*, **481**, 819
- Mikhalyaev, B. B., & Solov'ev, A. A. 2005, *Solar Phys.*, **227**, 249
- Moré, J. J., & Wright, S. J. 1993, *SIAM Frontiers Appl. Math.* 14: Optimization Software Guide (Philadelphia, PA: SIAM)
- Nakariakov, V. M., & Ofman, L. 2001, *A&A*, **372**, L53
- Nakariakov, V. M., Ofman, L., DeLuca, E. E., Roberts, B., & Davila, J. M. 1999, *Science*, **285**, 862
- Nakariakov, V. M., & Verwichte, E. 2005, *Living Rev. Solar Phys.*, **2**, 3, URL: <http://www.livingreviews.org/lrsp-2005-3> (cited on 2005-07-05)
- O'Shea, E., Srivastava, A. K., Doyle, J. G., & Banerjee, D. 2007, *A&A*, **473**, L13
- Ruderman, M. S., & Roberts, B. 2002, *ApJ*, **577**, 475
- Terradas, J., Arregui, I., Oliver, R., Ballester, J. L., Andries, J., & Goossens, M. 2008, *ApJ*, **679**, 161
- Terradas, J., & Ofman, L. 2004, *ApJ*, **610**, 523
- Terradas, J., Oliver, R., & Ballester, J. L. 2006, *ApJ*, **650**, L91
- Tomczyk, S., McIntosh, S. W., Keil, S. L., Judge, P. G., Schad, T., Seeley, D. H., & Edmondson, J. 2007, *Science*, **317**, 1192
- Van Doorselaere, T., Brady, C. S., Verwichte, E., & Nakariakov, V. M. 2008a, *A&A*, **491**, L9
- Van Doorselaere, T., Nakariakov, V. M., & Verwichte, E. 2007, *A&A*, **473**, 959
- Van Doorselaere, T., Nakariakov, V. M., & Verwichte, E. 2008b, *ApJ*, **676**, L73
- Van Doorselaere, T., Nakariakov, V. M., Young, P. R., & Verwichte, E. 2008c, *A&A*, **487**, 17
- Van Doorselaere, T., Ruderman, M. S., & Robertson, D. 2008d, *A&A*, **485**, 849
- Verth, G., & Erdélyi, R. 2008, *A&A*, **486**, 1015
- Verwichte, E., Foullon, C., & Nakariakov, V. M. 2006a, *A&A*, **449**, 769
- Verwichte, E., Foullon, C., & Nakariakov, V. M. 2006b, *A&A*, **452**, 615
- Verwichte, E., Nakariakov, V. M., Ofman, L., & DeLuca, E. E. 2004, *Solar Phys.*, **223**, 77
- Wang, T. J., & Solanki, S. K. 2004, *A&A*, **421**, L33
- Williams, D. R., et al. 2001, *MNRAS*, **326**, 428
- Wülser, J.-P., et al. 2004, *Proc. SPIE*, **5171**, 111